Multimodal assessment of mechanically induced transformation in metastable multi-phase steel using X-ray nano-tomography and pencil-beam diffraction tomography

Toda, Hiroyuki
Department of Mechanical Engineering, Kyushu University

Hirayama, Kyosuke
Department of Materials Science and Engineering, Kyoto University

Okamura, Kai
Department of Mechanical Engineering, Kyushu University

Suzuki, Takafumi
Department of Mechanical Engineering, Kyushu University

他

https://hdl.handle.net/2324/6792831

出版情報：Acta Materialia. 234 (1), pp.117956-, 2022-08. Elsevier
バージョン：

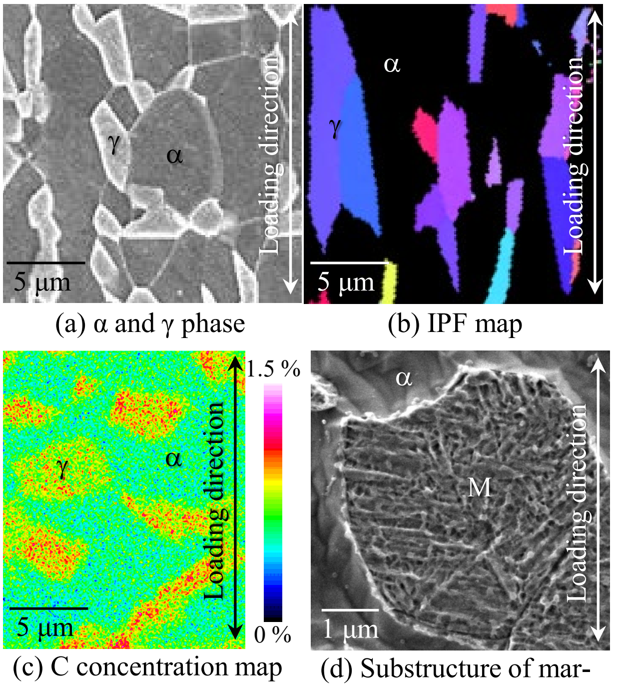

(a) α and γ phase
(b) IPF map
(c) C concentration map
(d) Substructure of martensite

Fig. S1. (a) Morphologies of ferrite and retained austenite phases (SEM), (b) details of the retained austenite grains (EBSD-IPF: color code is available in Fig. 2 as a form of [001] inverse pole figure), (c) carbon concertation distribution (EPMA), and (d) the substructure of martensite (EBSD).

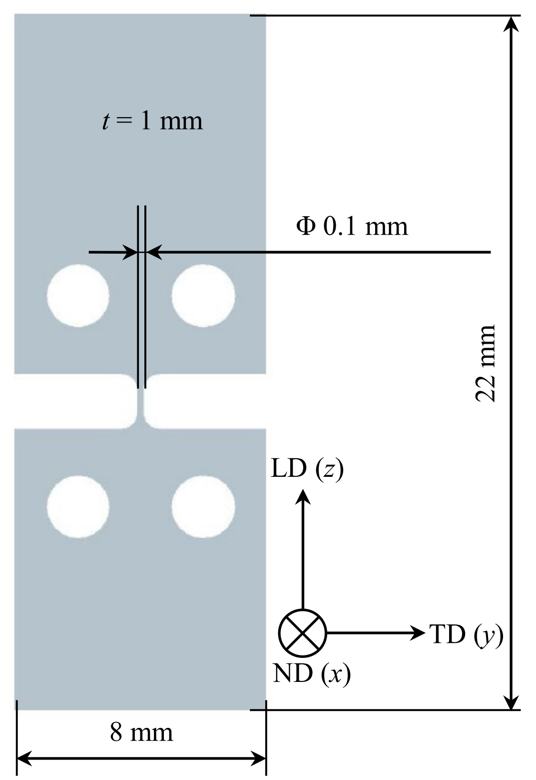

Fig. S2. Geometry of in-situ tensile test specimens that were common to both nano-tomography and pencil beam X-ray diffraction experiments.

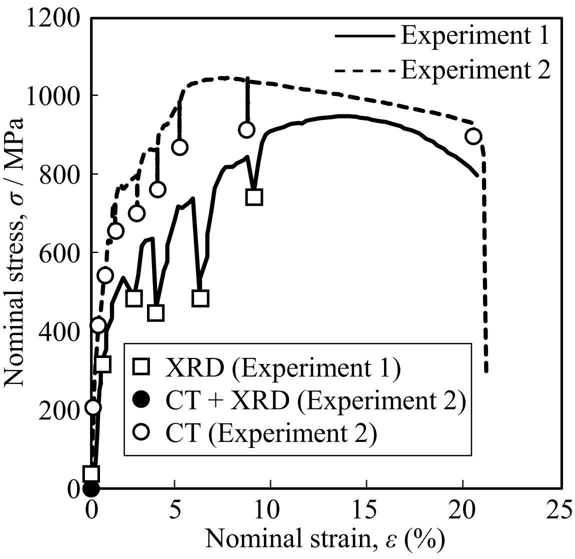

Fig. S3. Stress–strain curves recorded during the two in-situ tensile tests. Solid and dashed line show experiments 1 and 2, respectively.

Table S1 Major conditions for the synchrotron experiments.

Experiment	X-ray energy	Scintillator	Effective pixel size	Spatial resolution	Exposure time	Sample-to-detector distance
X-ray diffraction (Experiment 1)	37.7 keV	20-μm thick P43 ($Gd_2O_2S:Tb+$)	6.5 μm × 6.5 μm	19 μm	0.03 sec	20 mm
X-ray micro-tomography (Experiment 2)	20 keV	20-μm thick GAGG ($Gd_3Al_2Ga_3O_{12}$: Ce+)	0.5 μm × 0.5 μm	1.0 μm	0.15 sec	20 mm
X-ray nano-tomography (Experiment 2)	20 keV	200-μm thick LuAG ($Lu_3Al_5O_{12}:Ce+$)	0.061 μm × 0.061 μm	0.16 μm	0.5 sec	165 m

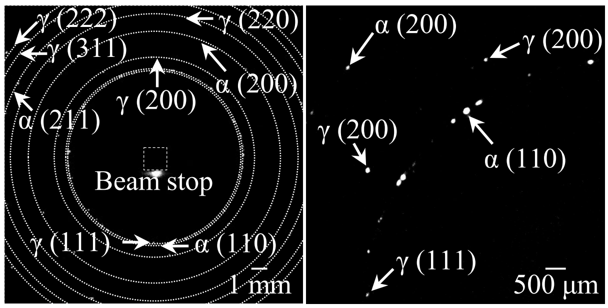

(a) The whole diffraction pattern with rings at $\varepsilon = 0$ %

(b) A part of the diffraction pattern at $\varepsilon = 0$ %

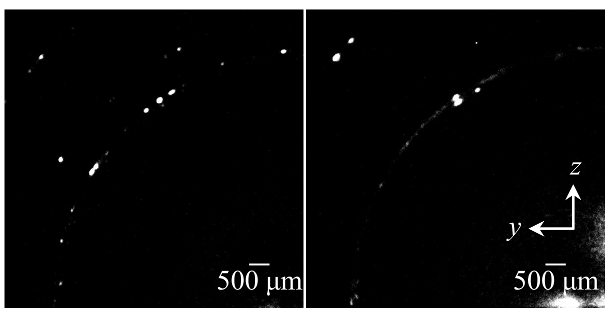

(c) A part of the diffraction pattern at $\varepsilon = 0.5$ %

(d) A part of the diffraction pattern at $\varepsilon = 2.3$ %

Fig. S4. Examples of X-ray diffraction patterns obtained in the pencil-beam X-ray diffraction experiments: (a) The whole diffraction pattern at $\varepsilon = 0$ % with rings at which the sum of squares of deviations from the diffraction spot data becomes minimal. (b) - (d) Parts of the diffraction patterns obtained at various applied strain levels in Experiment 1, demonstrating diffraction spots from a few crystallographic planes of the ferrite and retained austenite phases and their changes with applied strain.

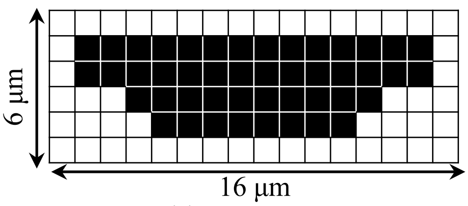

□ Beam positions

■ Beam positions at which a diffraction spot originated from a specific grain is observed

(a) Clustered diffraction spots at ω = 62º.

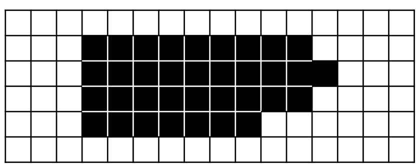

(b) Clustered diffraction spots at ω = 89º.

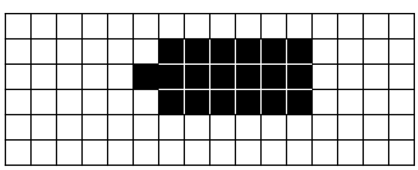

(c) Clustered diffraction spots at ω = 127º.

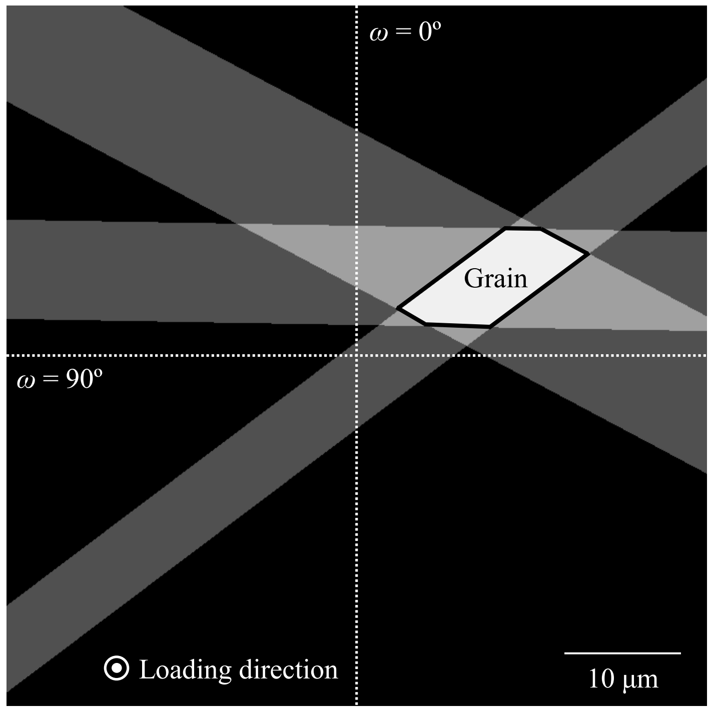

(d) Grain reconstruction from a set of the three clustered XRD spots shown in (a) – (c).

Fig. S5. (a) – (c) Examples of clustered X-ray diffraction spots for a specific grain that have been accumulated at the three specimen rotation angles, ω, during the raster scan data collection in Experiment 1. (d) is a crude reconstruction of grain morphology using the three diffraction spot clusters shown in (a), which can be assumed as pseudo projected images.

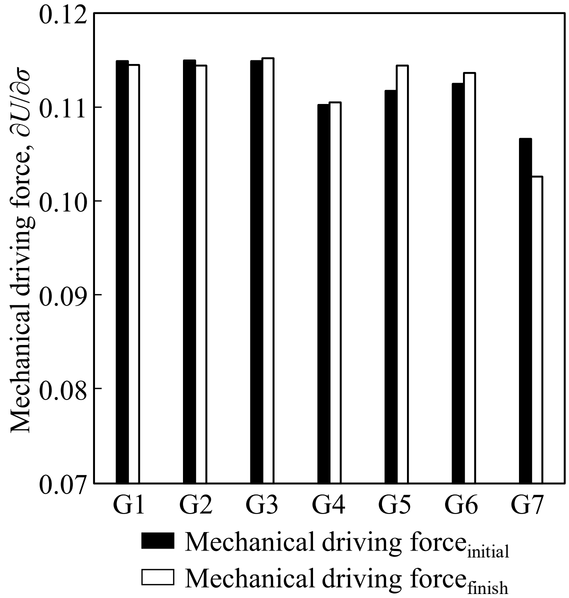

(a) Mechanical driving force

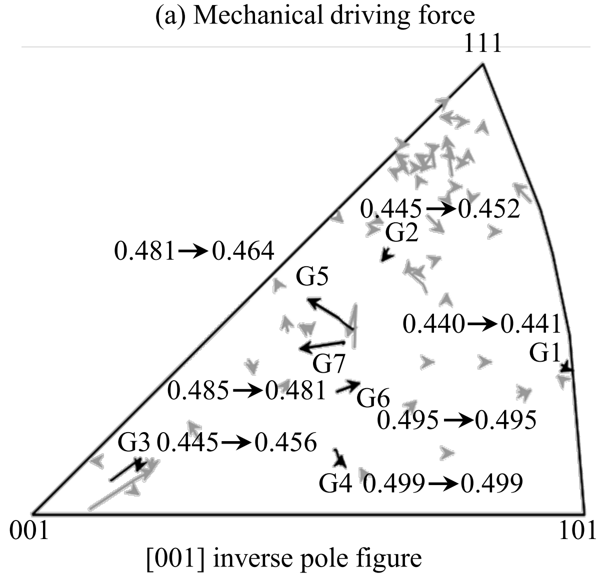

(b) Grain orientation and rotation

Fig. S6. (a) Mechanical driving force, U, for austenite-to-martensite transformation expressed as $\partial U/\partial\sigma$ and (b) crystallographic orientation distribution and rotation behavior on a [001] inverse pole figure for grains G1 - G7 shown in Fig. 9. The decimal pairs shown beside the individual grains in (b) represent the Schmid factor values before and after austenite-to-martensite transformation.

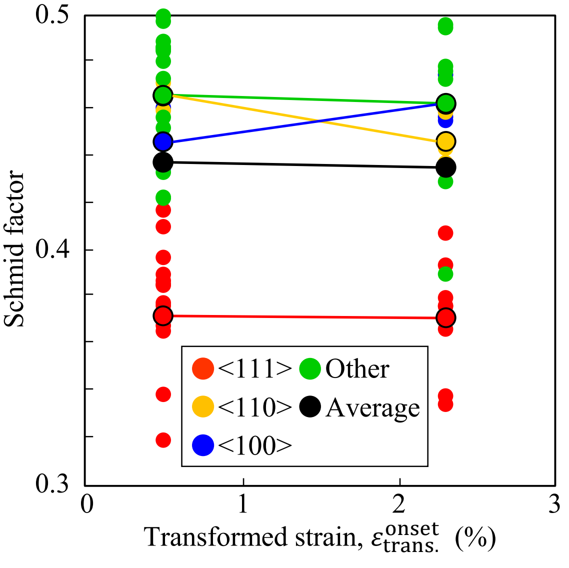

Fig. S7. Schmid factor before the onset of austenite-to-martensite expressed as a function of nominal strain at which transformation is started for each grain. All the 58 austenite grains, which have been successfully identified in Experiment 1, were classified according to initial grain orientations; orientations to the tensile axis within 15º from <111>, <110> and <100> directions, and the others, together with the average values for all the grains.